ACS OMEGA

Open Access

http://pubs.acs.org/journal/acsodf

Article

Highly Luminescent Eu^{3+}-Incorporated Zr-MOFs as Fluorescence Sensors for Detection of Hazardous Organic Compounds in Water and Fruit Samples

Karanika Sonowal, Sanmilan Jyoti Kalita, Siddhartha K. Purkayastha, Juri Goswami, Purashri Basyach, Riya Das, Abhishek Borborah, Ankur K. Guha, and Lakshi Saikia*

Cite This: *ACS Omega* 2024, 9, 2504−2518

Read Online

ACCESS | Metrics & More | Article Recommendations | Supporting Information

ABSTRACT: Considering the risk of toxic organic compounds to both human health and the environment, highly luminescent Eu^{3+}-incorporated amino-functionalized zirconium metal−organic frameworks, namely, Eu/MOF and Eu@MOF were synthesized via the solvothermal method. The synthesized luminescent europium-incorporated MOFs act as outstanding sensor materials for diphenylamine and dinitrobenzene detection in water and fruit samples. The synergistic effect of Eu^{3+} metal ions and amino-functionalized MOFs enhances the luminescent properties of the MOFs improving the fluorescence sensing ability toward the analytes. The enhancement in the detection capacity of the Eu^{3+}-incorporated sensors than the sole MOF toward toxic organic compounds was confirmed using the Stern−Volmer equation of limit of detection (LOD) measurements along with fluorescence lifetime measurements. The sensors exhibited turn-on fluorometric detection toward their respective analytes due to the inner filter effect. The plausible fluorescence sensing mechanism has been studied. The DFT calculations have been integrated to study the structure, stability, and charge transfer processes.

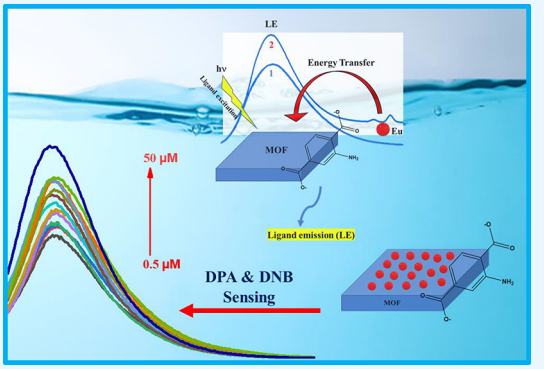

1. INTRODUCTION

Industrialization and population blasts have serious effects on the environment and its resources, causing several disasters such as air and water pollution. Environmental pollutants such as organic, inorganic compounds, and toxic gases cause severe health hazards to living beings. There are different water purification techniques such as adsorption, membrane-based techniques, and chemical and biological methods, among which the fluorescence-based sensing technique is one of the quickest, easiest, highly sensitive, and most accurate processes for toxic compounds sensing in water. A sensor is usually made of two components: sensing and transduction. The transduction component translates the sensed information into a different electrical or optical signal in the interaction of the sensor with analytes.[1−4] For an effective sensor, it should possess characteristics such as high selectivity, sensitivity, quick response time, stability, low cost, and reusability. In past decades, several carbonaceous materials, such as carbon nanotube, graphitic carbon nitride, graphene, activated charcoal, quantum dots, and so on, porous coordination polymers, such as MOFs, COFs, and zeolites, and different metal precursors and their sulfides, oxides, nitrides and so forth have been used for sensing of environmental pollutants.[5−13]

Organic aromatic compounds such as nitrobenzene are widely used in chemical production, such as pesticides, pharmaceuticals, aniline, dye, and commercial nitroaromatic explosives. However, the high accumulation of nitrobenzene in the environment causes severe security problems due to high toxicity and nondegradability. Nitrobenzene is a highly explosive volatile solvent and a basic component of nitroaromatic compounds. Therefore, it is necessary to identify and detect such hazardous explosives in environmental resources to protect human health and the environment. Modern analytical instrumentation techniques such as Raman spectroscopy, X-ray dispersion, ion mobility spectroscopy, gas chromatography−mass spectrometry (GC-MS), fluorescence spectrophotometry, and so on can be used to detect and quantify hazardous organic compounds.

Similarly, diphenylamine (DPA) is an antioxidant and is widely used for commercial purposes for storing apples. DPA is a derivative of aniline which prevents oxidation of α-farnesene for protecting apple skin from oxidation during long-time

Received: September 18, 2023
Revised: November 1, 2023
Accepted: November 7, 2023
Published: December 31, 2023

https://doi.org/10.1021/acsomega.3c07158
ACS Omega 2024, 9, 2504−2518

storage.[14,15] DPA controls the superficial scald of apples during postharvest treatment, which occurs via oxidation of α-farnesene, leading to damage of the outer layer cells of apples, browning of apple skin, and cell death. The maximum residue level of DPA in apples is 5 mg kg^{-1}.[6] Besides, DPA is widely used in industries for manufacturing plastic, dyes, photography chemicals, rubber, and pharmaceuticals. DPA-containing food leads to several health issues such as erythropoiesis, hemosiderosis, bladder disease, hypertension, and so on.[16] Considering the use of DPA as a food preservative, it is very important to determine the risk level of DPA in fruits. Several methods have been employed to date to detect and quantify DPA such as spectrophotometric, fluorometric, electrochemical, gas chromatography−mass spectrometry, and high-performance liquid chromatography.[15]

Among various modern analytical techniques, the fluorescence-based technique is one of the most promising sensing methods for diphenylamine and dinitrobenzene detection in water, owing to its sensitivity and simplicity. Metal−organic frameworks (MOFs) are used on a large scale for identifying and highly selective and sensitive detection of hazardous materials in air and water media due to uniform porosity, tunability, tailorable structure, and unique fluorescent properties. Additionally, MOF-based luminescent chemosensors exhibit high sensitivity, quick response, strong luminescence, stability, and reusability. The major components of an MOF for generating excellent luminescence properties are the metal components and organic ligands with luminophores and conjugated π-systems. Luminescent MOFs are considered excellent chemical sensors for their easy tunability and unique porosities that provide host−guest interactive sites for the selective sensing of guest molecules. Lanthanide metal−organic frameworks (Ln-MOFs) are drawing the major attention of researchers owing to their strong emissions and longer lifetime. Ln-MOFs are mostly considered for sensing applications due to their strong optical properties generated from 4f electrons.[36−40] Some Ln-MOFs exhibit characteristic fluorescence emissions due to intrinsic 4f−4f electronic transitions of lanthanide ions,[17−21] and most of them exhibit fluorescence due to the "antenna effect" depending on their high color purity and large Stokes shifts.[22,23] Fabricating Ln-MOF-based sensors for toxic element and compound detection involves the use of Π-conjugated aromatic linkers with available interactive sites where the extended conjugated system with available luminophores acts as an antenna for light energy absorption and excitation energy transformation to the active lanthanide metal centers for exhibiting strong luminescence.[24−26] Available interactive sites such as open metal sites and Lewis sites can effectively interact with the incoming guest molecules or foreign materials, executing selective sensing ability. The structural, physical, and chemical changes in MOFs may occur during the adsorption of guest molecules upon sensing experiments which have prompted the applicability of MOFs for environmental contaminant sensing in recent years.[27] Basically, MOFs containing transition metal ions execute linker-based emissions rather than metal-centric emissions. However, Ln-MOFs strongly exhibit metal-centric emissions through the antenna effect. Doping or loading small concentrations of lanthanide metal ions on pristine MOFs enhances the luminescent properties of MOFs to sense guest molecules around their environment, also providing host−guest interactive sites to concentrate more guest molecules in the uniform pores of MOFs to enhance the detection sensitivity. Probing ultratrace level analytes with high accuracy and sensitivity using MOF-based sensors is highly demanded for its commercialization and environmental benefits.

In this regard, we have synthesized one Eu^{3+}-incorporated NH_2-functionalized Zr-MOF for probing toxic materials in water and fruit samples to protect human health. The synthesized binary composite has been reported for the first time with different synthetic methodologies for the selective sensing of hazardous organic compounds with good detection sensitivity. Eu^{3+} loading on the MOF surface enhances the optical properties of Zr-MOF leading to enhanced detection capability of toxic organic compounds such as dinitrobenzene (DNB) and diphenylamine (DPA) for environmental remediation. The binary composites were effectively used for DPA detection in apple extract samples and DNB detection in industrial water samples. The binary composites act as efficient sensors for hazardous organic compound detection with high sensitivity and good detection capacity even in very few composite concentrations.

2. SYNTHESES AND CHARACTERIZATIONS

2.1. Synthesis of Eu/MOFs. Eu^{3+}-incorporated NH_2-functionalized Zr-MOFs, Eu/MOFs, were synthesized via the ex-situ solvothermal method. $Eu(NO_3)_3.5H_2O$ (0.1 mmol; 0.043 g) and 0.1 mmol (0.172 g) NH_2−UiO-66 MOF was taken in a 50 mL beaker, and 30 mL of *N*,*N*-dimethylformamide (DMF) was added into it followed by the addition of one drop of concentrated hydrochloric acid (HCl). The mixture was stirred properly for 1 h for good dispersion of the solution. Then, the solution was transferred into an autoclave, and the autoclave was sealed properly. The reaction was set at a temperature of 160 °C for 24 h, and after the completion of the reaction, the autoclave was allowed to cool to room temperature. Then, the solid product obtained was filtered and washed several times with DMF and acetone. The light yellowish powder product obtained was dried in a vacuum.

$$Eu(NO_3)_3 5H_2O + NH_2 - UiO - 66 \xrightarrow[DMF,\ conc.\ HCl]{160^\circ C,\ 24\ h} Eu/MOF$$

2.2. Synthesis of Eu@MOF. Eu^{3+}-incorporated NH_2-functionalized Zr-MOFs, Eu@MOFs, were synthesized via the in situ solvothermal method. 0.1 mmol (0.043 g) $Eu(NO_3)_3.5H_2O$, 1 mmol (0.181 g) 2-amino-terephthalic acid (NH_2−BDC), and 1 mmol (0.233 g) zirconium tetrachloride ($ZrCl_4$) were taken in a 50 mL beaker, and 30 mL of *N*,*N*-dimethylformamide (DMF) was added followed by the addition of one drop of concentrated hydrochloric acid (HCl). The solution was stirred at room temperature for 1 h for good dispersion of the reactant precursors and then transferred into an autoclave. The tightly sealed autoclave was set at 160 °C for 24 h, and after the completion of the reaction, it was allowed to cool to room temperature. The light yellowish solid product obtained was filtered, washed several times with DMF and acetone, and dried in a vacuum.

2.3. Complete Material Synthesis.

$$Eu(NO_3)_3 5H_2O + ZrCl_4 + NH_2 - BDC \xrightarrow[DMF,\ conc.\ HCl]{160^\circ C,\ 24\ h} Eu@MOF$$

https://doi.org/10.1021/acsomega.3c07158
ACS Omega 2024, 9, 2504−2518

The details of NH_2−UiO-66 MOF synthesis and some other characterizations are provided in Appendix A Supplementary Data.

2.4. General Method of Fluorescence Measurements. The fluorescence readings were taken using a FLUOROLOG-3 fluorescence spectrophotometer. Fluorescence intensities for diphenylamine (DPA) and dinitrobenzene (DNB) detection in water were taken using 40 μL of 0.2 mg/mL synthesized MOF materials in a cuvette. After that, 40 μL of freshly prepared 12 different concentrated solutions of analytes (0.5−50 μM) were mixed accordingly, and the total volume was covered up to 3 mL with distilled water. Then, the cuvette was placed inside the instrument for fluorescence measurements. The fluorescence readings were taken at a 365 nm excitation wavelength, and the slits were set at 5 nm. To check the selectivity of the sensors toward the analytes, fluorescence measurements were performed with some other organic compounds (50 μM) in distilled water following similar procedures. Real samples were analyzed with five different spiked concentrations of DPA and DNB by the standard addition method (Tables 1 and 2).

Table 1. Elemental Compositions of the Synthesized Materials with Their Atomic Percentage

sl no.	MOF materials	atomic %				
		O 1s	C 1s	N 1s	Zr 3d	Eu 3d5
1	parent MOF	30.63	60.56	5.09	3.71	
2	Eu/MOF	32.89	57.49	4.94	3.8	0.88
3	Eu@MOF	31.55	58.55	5.66	4.22	0.01

Table 2. Fluorescence Sensing Study with the Industrial Water Sample[a]

samples	sensor	added [DNB] (μM)	found [DNB] (μM)	recovery (%)	RSD (%)
industrial water	Eu/MOF	0.5	0.45	94.2	0.02
		5	5.05	87.74	0.01
		15	14.26	85.84	0.05
		25	23.50	96.87	0.04
		35	35.69	94.52	0.07
	Eu@MOF	0.5	0.4	108.2	0.04
		5	5.26	107.3	0.05
		15	13.27	103.6	0.01
		25	24.69	92.1	0.02
		35	34.57	89.8	0.04

[a]The results are executed as mean value of three measurements.

2.5. Real Samples and Their Pretreatment. The real samples used were industrial water and the aqueous apple extract of the outer layer. The industrial water samples were pretreated before being subjected to fluorescence analysis. The industrial water sample was filtered first using a 0.25 μm poly(ether sulfone) (PES) membrane syringe filter (UNIFLO, Whatman, UK) for removing large contaminants. The microfiltration process was repeated two times, and the water was evaporated before performing fluorescence analysis to kill microbes present in the water and also to remove other volatile contaminants in water. Thereafter, the fluorescence readings for the sensor with spiked analytes were monitored. However, there is a high possibility of microorganism contamination in wastewater and they may absorb ultraviolet (UV) light that can produce background fluorescence under UV excitation during photoluminescence (PL) analysis. Therefore, pretreatment is highly required before performing fluorescence analysis in industrial water samples.

Apples were bought from a nearby market to prepare an aqueous apple extract sample. Apples were first washed with distilled water and then boiled in distilled water to soften the outer layer of the apple so that diphenylamine (DPA) dissolves in water. However, the solubility of DPA is less in water; therefore, the solution containing apple was heated for 24 h. The DPA content in the aqueous apple extract obtained was confirmed from spectrophotometric and high-resolution mass spectrometry (HRMS) analysis.

3. RESULTS AND DISCUSSION

Considering the higher light absorption capability of the amino-functionalized Zr-MOF containing strong luminescent Eu (III) metal ions, the Eu^{3+}-incorporated NH_2−UiO-66 MOF has been used as a fluorescence-based sensor for sensing toxic organic compounds in fruit and industrial water samples. The structural integrity of the synthesized Eu/MOF and Eu@MOF remains intact as that of the parent NH_2−UiO-66 MOF, which was confirmed from PXRD measurements as shown in Figure 1a. No extra peaks for Eu^{3+}-incorporated Zr-MOFs were observed due to the very small content of loaded Eu^{3+} metal ions. The intense diffraction peaks of the europium-incorporated MOFs at 7.35, 8.52, 25.58, 30.75, 43.41, and 50.23° are in good agreement with the simulated NH_2−UiO-66 MOF.[28] The crystallite size of the synthesized MOFs was calculated using the Debye−Scherrer

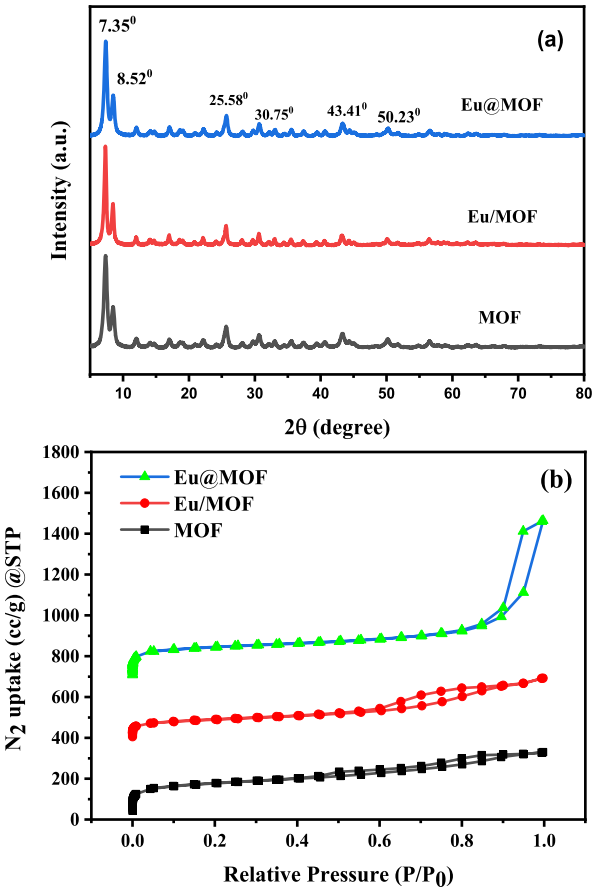

Figure 1. (a) PXRD measurements of the synthesized MOF and (b) N_2 adsorption−desorption isotherm curves for the synthesized materials.

https://doi.org/10.1021/acsomega.3c07158
ACS Omega 2024, 9, 2504−2518

equation and was found to be 6.57 nm for the MOF, Eu/MOF, and Eu@MOF. The unique porosities of the synthesized MOFs were confirmed by the N_2 adsorption−desorption isotherm. The Eu^{3+}-incorporated MOFs, Eu/MOF and Eu@MOF exhibited a BET surface area of 401 and 400 m^2/g, respectively, which is lower than that of the parent MOF with a surface area of 582 m^2/g (Figure 1b). The decrease in the surface area of Eu^{3+}-incorporated MOFs is due to the presence of europium metal ions on the MOF's surface. The similar pore width of 1.4 nm of the synthesized MOF materials confirms the microporous nature of the materials.

X-ray photoelectron spectroscopy (XPS) analysis reveals that the Eu^{3+}-incorporated MOF materials (Eu/MOF and Eu@MOF) exhibit similar binding energy values of 283.4 and 287.3 eV for C 1s; 398.0 eV for N 1s and 530.4 eV for O 1s (Figure 2a−c,f−h); 181.4 eV for Zr $3d_{3/2}$; and 183.7 eV for Zr $3d_{5/2}$ (Figure 2e,j). Eu/MOF exhibits two binding energy values at 1124.2 and 1154.2 eV that correspond to Eu^{2+} $3d_{5/2}$ and Eu^{2+} $3d_{3/2}$, respectively. While the peaks of Eu/MOF at 1134.5 and 1164.0 eV represent Eu^{3+} $3d_{5/2}$ and Eu^{3+} $3d_{3/2}$, respectively (Figure 2d), Eu@MOF exhibits binding energy values of 1123.5 and 1154.6 eV that correspond to Eu^{2+} $3d_{5/2}$ and Eu^{2+} $3d_{3/2}$, respectively. The peaks at 1134.9 and 1163.7 eV represent Eu^{3+} $3d_{5/2}$ and Eu^{3+} $3d_{3/2}$, respectively (Figure 2i). The photoelectron lines for Eu 3d of both europium-incorporated MOFs confirm the presence of both (+2/+3) oxidation states of europium metal ions with highly intense Eu^{3+} XPS spectral peaks. The survey reports for the synthesized MOF materials are shown in Figure 2k. The elemental compositions of the synthesized materials with their atomic percentage are listed in Table 1.

The morphological studies were performed using SEM and TEM analysis. The morphology of the Eu/MOF and Eu@MOF is similar to that of the parent MOF, which has been confirmed from SEM analysis (Figure 3a−c). TEM images (Figure 3d) of the Eu@MOF confirm the cubic morphology of the MOF. Figure 3e−g are the HRTEM images of Eu@MOF at 10, 10, and 5 nm resolution, respectively which confirms the presence of uniformly distributed highly crystalline lattice fringes of Eu^{3+} metal ions on the porous MOF surface. Figure 3h, i represents the HRTEM of Eu@MOF at 5 nm resolution with a crystalline lattice parameter of 0.309 nm that signifies the presence of cubic phase Eu_2O_3 in Eu@MOF which matches some previous reports.[29,30] TEM images, Figure 3j,k, of Eu/MOF confirm the intact cubic morphology of the MOF. Figure 3l is the HRTEM of Eu/MOF at 5 nm resolution, which shows a uniform distribution of Eu^{3+} metal ions on the MOF surface with crystalline lattice planes of 0.309 nm with cubic phase Eu_2O_3 without other phases. The distinct lattice planes for Eu^{2+} could not be observed from TEM analysis due to their very less percentage as compared to Eu^{3+} states. Therefore, Eu^{3+} is the dominant oxidation state in both europium-incorporated MOFs. Energy-dispersive X-ray (EDX) analysis (Figure S1) of Eu/MOF and Eu@MOF confirms the presence of C, N, O, Zr, and Eu in the Zr-MOF. The insets of Figure 3d,j are SAED patterns for Eu@MOF and Eu/MOF, respectively, which confirm the highly crystalline nature of the europium-incorporated MOFs.

The photophysical properties of the synthesized MOF materials were studied by using UV−vis and fluorescence spectrophotometric analysis at room temperature. The sole MOF and Eu^{3+}-incorporated MOFs exhibit a similar absorbance at 265 and 365 nm as shown in Figure 4a; the absorption peak at 265 nm is due to the presence of Zr-oxo clusters in MOFs, and

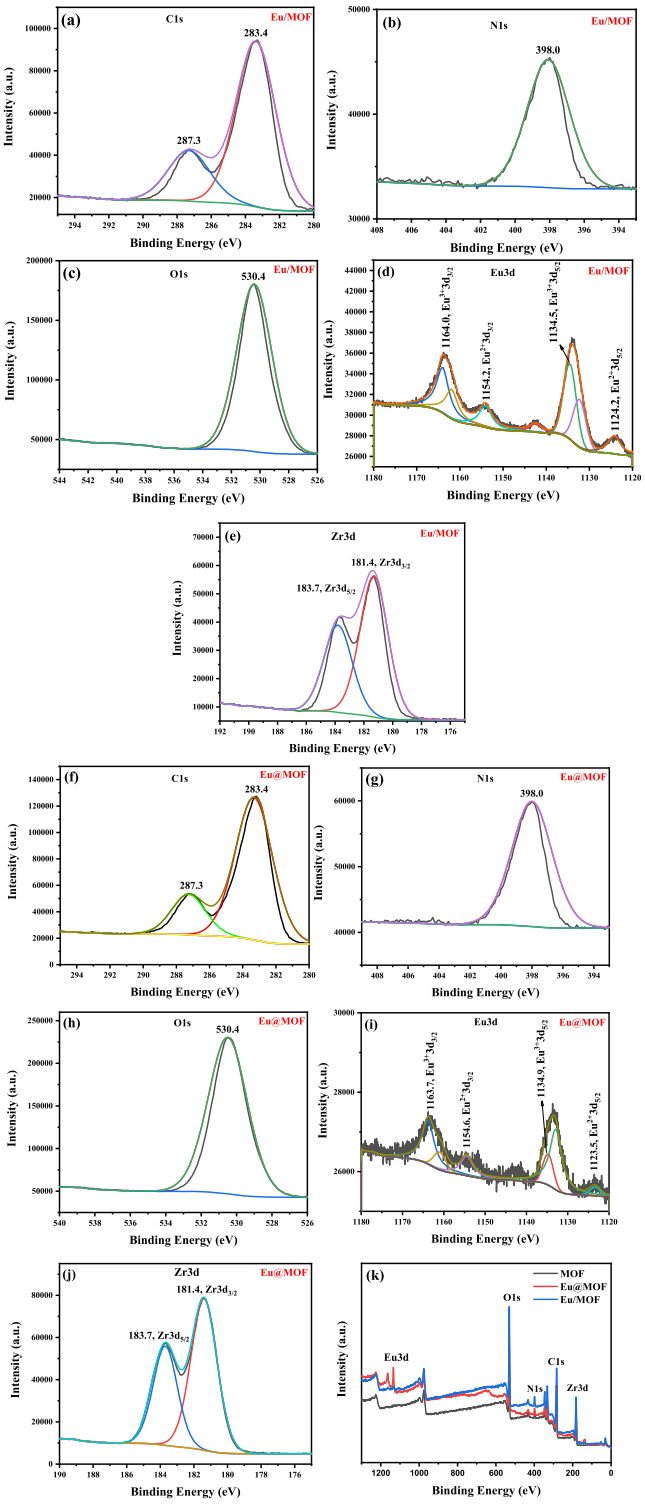

Figure 2. (a−c) XPS spectra of Eu/MOF for C 1s, N 1s, and O 1s, respectively; (f−h) XPS spectra of Eu@MOF for C 1s, N 1s, and O 1s, respectively; (e, j) XPS spectra for Zr 3d of Eu/MOF and Eu@MOF, respectively; (d, i) XPS spectra for Eu 3d of Eu/MOF and Eu@MOF, respectively; and (k) survey report of the synthesized MOF materials.

the peak at 365 nm corresponds to ligand to metal charge transfer (LMCT) in the Zr-MOF. No new absorption peak of europium at 300 nm in Figure 4a for Eu/MOF and Eu@MOF could be observed due to its very low content on the MOF surface. The parent NH_2−UiO-66 MOF exhibits strong blue

https://doi.org/10.1021/acsomega.3c07158
ACS Omega 2024, 9, 2504−2518

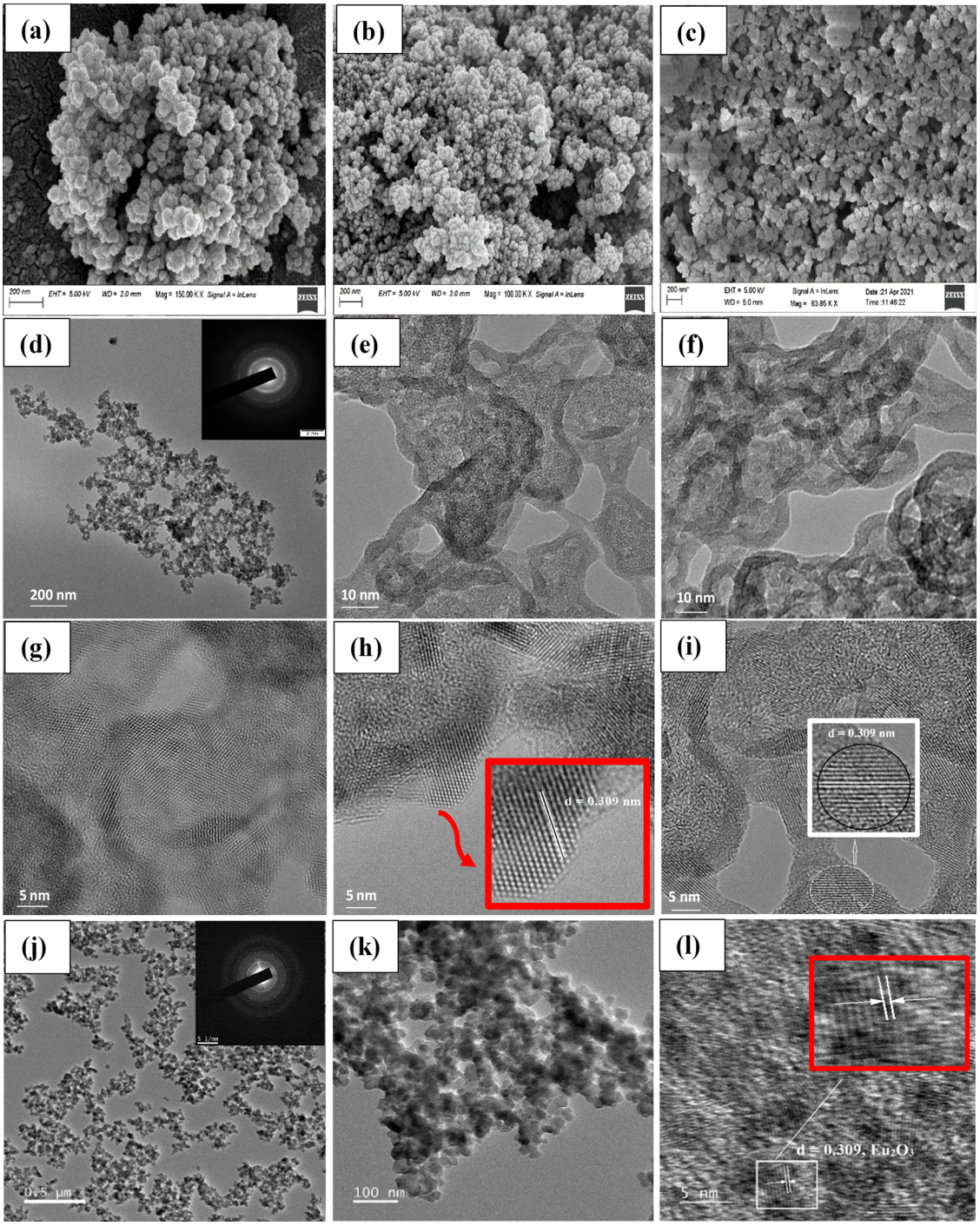

Figure 3. (a−c) are the SEM images for MOF, Eu@MOF, and Eu/MOF, respectively; (d−i) TEM and HRTEM images of Eu@MOF; (j−l) TEM and HRTEM of Eu/MOF. The insets in Figure 3d and j are the SAED patterns for Eu@MOF and Eu/MOF, respectively.

fluorescence in the range of 430−440 nm at an excitation of 365 nm (Figure 4b). The two Eu^{3+}-incorporated MOFs exhibited strong blue fluorescence at a similar wavelength as that of parent MOF at 365 nm excitation wavelength along with two other small emission peaks at 592 nm (Eu^{3+}, $^5D_0$----^7F_J, $J = 0-4$) and 617 nm (Eu^{3+}, $^5D_0$----$^7F_2$), while using 1 mL of 0.2 mg/mL prepared MOF solutions. The inset of Figure 4b shows strong blue fluorescence emissions of the MOF, Eu/MOF, and Eu@MOF and slight red emission for Eu^{3+} metal ions under UV lamp irradiation at 365 nm. The strong fluorescence emissions in europium-incorporated MOFs at 440 nm as compared to direct europium metal emissions are due to light absorption by the amino group linked to benzene dicarboxylate in the Zr-MOF and re-emissions, which are more prominent as compared to Eu^{3+} emissions due to very low content of loaded Eu^{3+} metal ions and dominant characteristics of ligand to metal charge transfer (LMCT) from the $-NH_2$-linked Π-conjugated system to zirconium(IV) metal ion in the Zr-MOF; therefore, strong blue fluorescence emissions could be seen. Besides, Eu^{3+}-MOF interactions enhance the luminescence of the MOFs enhancing detection sensitivity. The strong fluorescence emissions signify that electron−hole pairs can be sufficiently created and

https://doi.org/10.1021/acsomega.3c07158
ACS Omega 2024, 9, 2504−2518

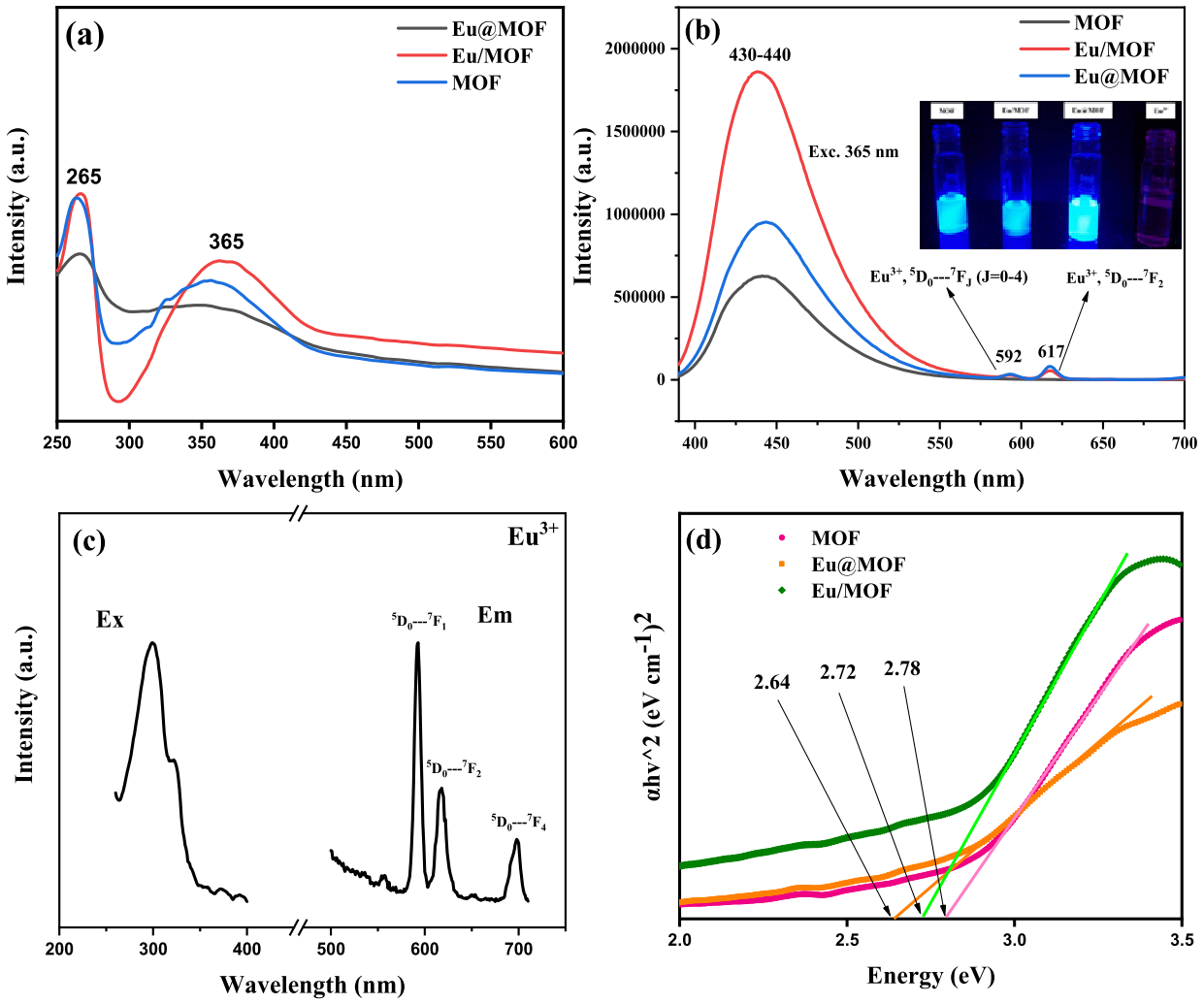

Figure 4. (a) UV−vis spectra for MOF, Eu/MOF, and Eu@MOF; (b) photoluminescence spectra for the synthesized MOFs, the inset is the strong fluorescence emission images for MOF, Eu/MOF, Eu@MOF, and Eu^{3+} metal ions, respectively; (c) fluorescence excitation−emission spectra for Eu^{3+}; (d) Tauc plot for band gap calculation.

separated upon photon absorption by the MOFs. The fluorescence emissions by the Eu^{3+}-incorporated MOFs are more intense as compared to the parent MOFs at a similar concentration (0.2 mg/mL) due to the synergistic effect of highly luminescent Eu^{3+} metal ions with sole MOFs on their surface. The lanthanide transitions are entirely metal-centric due to weak interaction with ligands and a large spin−orbit coupling value. Besides, 4f−4f transitions are strongly forbidden and the direct excitation of 4f orbitals is very weak; therefore, indirect excitations of the 4f orbital through the "antenna effect" is a possibility to excite the lanthanide center via energy transfer. In this study, the lanthanide metal emission is very less as could be seen from fluorescence measurements (Figure 4b) due to a very small percentage of Eu^{3+} metal ions, and hence, the antenna effect is almost insignificant in this study. It could be seen from the band energy diagram of the MOF and lanthanide metal ion that the conduction band (CB) energy of the Eu^{3+} metal is slightly more negative (−0.46 eV) than that of the sole MOF (−0.43 eV) executing the possibility of energy transfer from the CB of the Eu^{3+} metal to the sole MOF, which results in increasing the luminescence properties of the MOF via the lanthanide metal-MOF interaction as shown in Figure 6b. Hence, instead of the antenna effect, there is the possibility of Eu^{3+} metal to ligand back-donation of electrons, which could be observed in the system. Figure 4c is the excitation−emission spectra of Eu^{3+} metal ions which exhibit excitation at 300 nm and emissions at 592, 617, and 698 nm that correspond to three electronic transitions of europium metal at $^5D_0$—$^7F_1$, $^5D_0$—$^7F_2$, and $^5D_0$—$^7F_4$, respectively, which matches the previous reports.[31] The band gap of Eu^{3+}-incorporated MOFs decreases as compared to the parent MOF as confirmed by diffused-reflectance UV−vis spectrometry (Figure 4d). The band gap energies for MOF, Eu/MOF, and Eu@MOF are 2.78, 2.72, and 2.64, respectively.

The fluorescence lifetime of the synthesized MOFs was measured (Figure 5) and it was found that the fluorescence lifetime values for Eu@MOF (8.09 ns) and Eu/MOF (5.96 ns) are higher as compared to those of the parent NH_2−UiO-66 MOF (1.65 ns). This confirms that the incorporation of Eu^{3+} metal ions into Zr-MOF enhances the fluorescence lifetime of the Eu^{3+}-incorporated MOFs due to slow electron−hole pair recombination which enhances their luminescent properties for a longer period.

The Mott−Schottky analysis of the synthesized MOFs was conducted to know the electronic band structures and the conductive types of the materials, as shown in Figure 6a. The

https://doi.org/10.1021/acsomega.3c07158
ACS Omega 2024, 9, 2504−2518

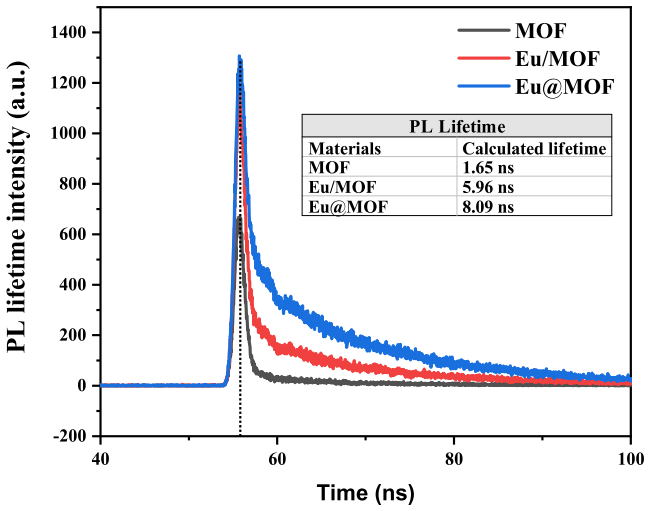

Figure 5. Time-resolved photoluminescence spectra of the synthesized MOFs.

MOFs exhibit negative flat-band potentials (V_{fb}) of −0.58, −0.47, and −0.34 V for MOF, Eu@MOF, and Eu/MOF, respectively, and negative flat-band potentials confirm the n-type semiconducting nature of the MOFs. The little decrease in V_{fb} for Eu@MOF and Eu/MOF as compared to the sole MOF confirms the formation of an active hybrid interface in the Eu^{3+}-incorporated MOF materials. As the conduction band energy levels of semiconducting materials are highly negative by 0.15 V than the flat-band potential, the conduction band positions for MOF, Eu@MOF, and Eu/MOF were calculated to be −0.43, −0.32, and −0.19 eV, respectively. The Mott−Schottky plots were measured by using 0.5 M aqueous Na_2SO_4 solution at a frequency of 1000 Hz with a calomel electrode as a reference electrode. The diffused-reflectance UV−vis spectra for the Eu^{3+} metal ion exhibit a band gap of 5.23 eV. The flat-band potential and conduction band energy for Eu^{3+} metal ions were found to be −0.61 V and −0.46 eV, respectively (Figure S2). The conduction band (CB) positions of Eu^{3+} metal ions (−0.46 eV) almost lie in equal energy levels as that of the parent MOF (−0.43 eV) as shown in Figure 6b. Besides, the CB of Eu^{3+} seems to be slightly more negative than the MOF. Therefore, it is presumed that there is a possibility of energy transfer from the highly luminescent Eu^{3+} metal center to the CB of the MOF that enhances the luminescence properties of the Eu^{3+}-MOF heterojunction for better detection capability.

Eu^{3+} incorporation in the Zr-MOF even in small loading enhances the optical properties of the MOF without changing the structural integrity of the Zr-MOF, which is confirmed by XRD analysis and fluorescence measurements. The main reason

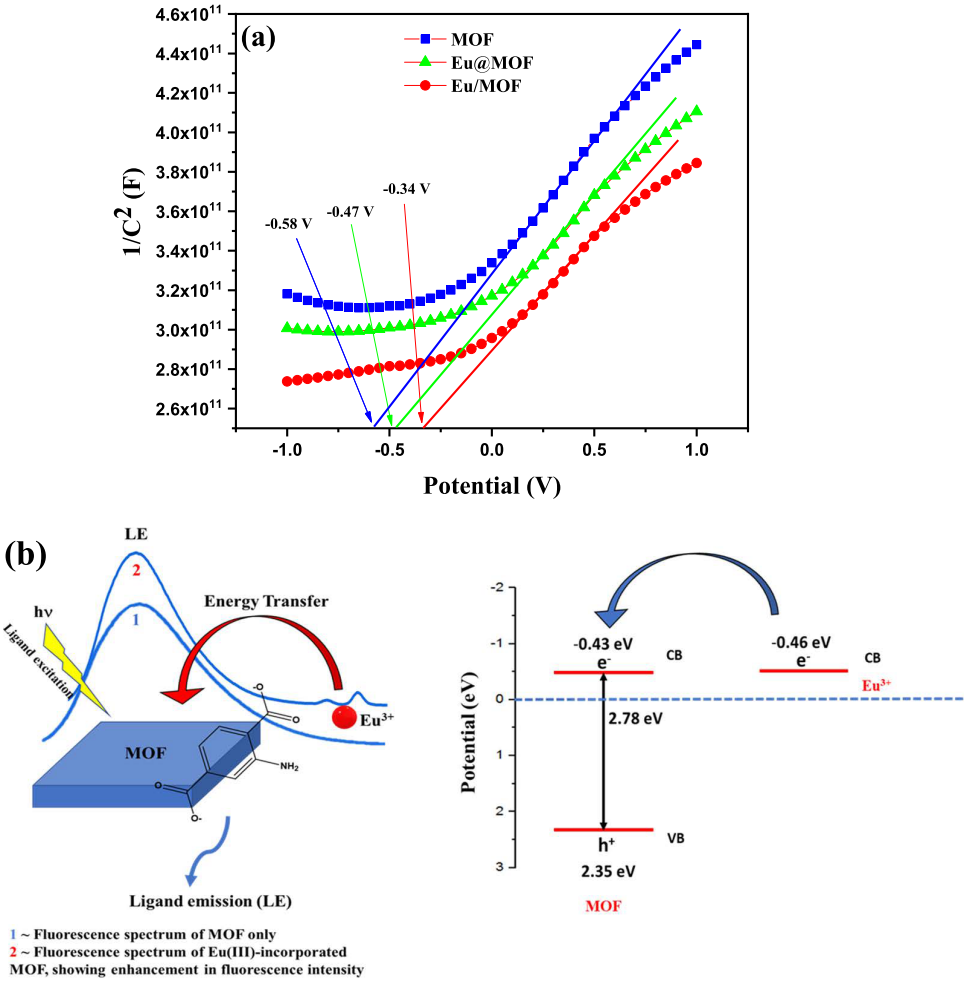

Figure 6. (a) Mott−Schottky plots for the MOF, Eu/MOF, and Eu@MOF; (b) Band energy diagram and schematic representation of the energy transfer process from the lanthanide metal ion to the MOF, showing luminescence enhancement of Eu^{3+}−MOF interaction.

https://doi.org/10.1021/acsomega.3c07158
ACS Omega 2024, 9, 2504−2518

for the enhancement in the optical properties is the highly luminescent nature of the Eu^{3+} ion, which occurs due to their partially filled 4f shell lying at a lower energy level than 5s and 5p shells that shield the 4f shell from the ligand environment. Considering the highly fluorescent nature of the Eu^{3+}-incorporated MOFs, the synthesized MOFs have been used as fluorescence sensors for the detection of hazardous organic compounds in water and fruit samples. The pH values of the synthesized materials are found to be 4.23, 5.52, and 4.65 for MOF, Eu/MOF, and Eu@MOF, respectively, which are acidic in nature, and the sensing activities were performed without adding any extra acids or bases or buffer solutions.

3.1. Computational Details. The europium-incorporated zirconium-based metal−organic framework MOF (Eu^{3+}-incorporated NH_2-functionalized Zr-MOF) such as Eu/MOF was fully optimized using hybrid functional PBE0[32] with a relativistic small-core effective core-potential basis set of Stuttgart/Dresden (SDD)[33] for the Zr and Eu atoms, while the 6-31+G* basis set for all other atoms. All these calculations were performed using the GAUSSIAN16 suite of programs.[34] Projected density of states (PDOS) has been calculated using the Multiwfn program code.[35]

Figure 7 shows the optimized geometries of the zirconium-based metal−organic framework MOF, (NH_2−UiO-66(Zr)) and the heterojunction Eu^{3+}−NH_2−UiO-66(Zr). The calculated binding energy is −0.32 eV, indicating that loading Eu^{3+} on NH_2−UiO-66 results in a stable complex.

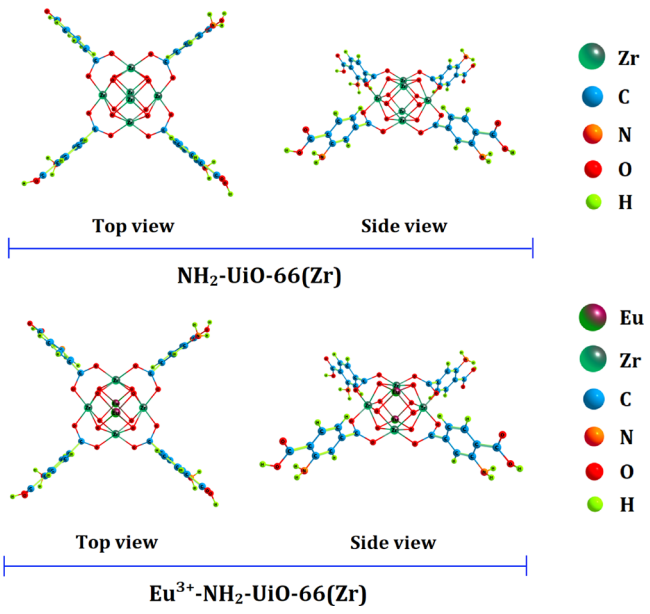

Figure 7. Optimized geometries of the NH_2−UiO-66(Zr) and Eu^{3+}−NH_2−UiO-66(Zr) heterojunction.

To get a better insight into the sensing ability of the Eu^{3+}-incorporated MOF, we have calculated the projected density of states of the Eu^{3+} loaded material (Figure 8). It is evident from Figure 8 that 4f electrons of Eu^{3+} are more dominant around the Fermi level which results in more charge transfer from Eu^{3+} to the conduction band of NH_2−UiO-66(Zr), enhancing the luminescence properties.

3.2. Sensing Activity Using Synthesized MOFs. The sensing activity was studied under room temperature conditions using the synthesized Eu^{3+}-incorporated MOFs and parent MOFs. A stock solution of diphenylamine (1000 μM) was

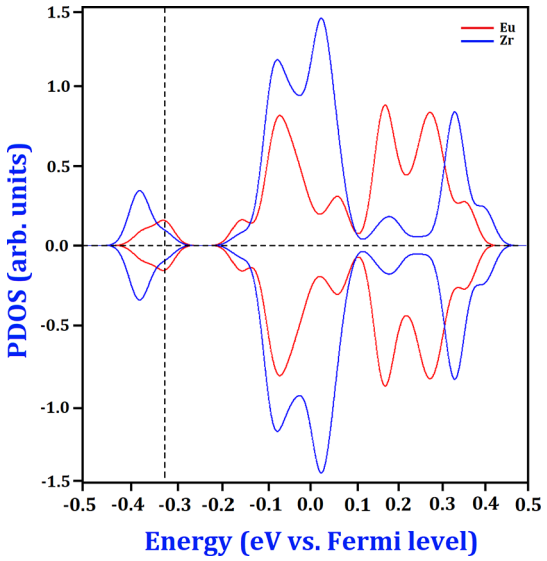

Figure 8. Representation of the partial density of states (PDOS).

prepared and by dilution method, 12 different concentrated solutions from 0.5 to 50 μM of diphenylamine (DPA) and dinitrobenzene (DNB) were prepared in distilled water. With the increasing amounts of spiked DPA and DNB concentrations, the fluorescence intensity of the synthesized MOFs increases gradually in the presence of the analytes, which confirms the turn-on fluorometric detection of DPA and DNB by the sensor. The fluorescence sensing effect was studied using the Stern−Volmer equation, and the limit of detection (LOD) was measured. The synthesized materials MOF, Eu/MOF, and Eu@MOF exhibited excellent detection capacity for DPA in water with LOD values of 0.842, 0.698, and 0.752 ppm, respectively, with good linearity (Figure 9). The Eu/MOF exhibited better detection capacity for DPA than Eu@MOF and parent MOF. Eu^{3+} incorporation in the Zr-MOF enhances the luminescent nature of MOFs, which results in an increment of detection capacity for DPA in water by Eu^{3+}-incorporated MOFs.

Similarly, the synthesized materials exhibited excellent detection capability for dinitrobenzene (DNB) in water by a fluorescence sensing method at an excitation of 365 nm. The Stern−Volmer plots for DNB sensing exhibited good linearity for sensing applications with a limit of detection of 0.909, 0.851, and 0.652 ppm for MOF, Eu/MOF, and Eu@MOF, respectively (Figure 10). The Eu@MOF exhibited better detection capacity for DNB than the Eu/MOF and parent MOF. The enhanced detection sensitivity of Eu^{3+}-incorporated MOFs rather than the parent MOF is due to the Eu^{3+}-MOF interaction that enhances the luminescent sensing activity toward the analytes on the porous MOF surface.

The error bar diagrams for the sensing activity are provided in Figures S6 and S7 of Appendix A Supplementary Data.

The Eu^{3+}-incorporated MOFs act as effective sensors for the sensitive detection of DPA and DNB in water. To check the selectivity of the sensors toward DPA and DNB detection, fluorescence sensing activity was tested with some other spiked organic compounds such as aniline derivatives and nitrobenzene derivatives as selective detection interfering substances, respectively, to better reflect selectivity. Aniline derivatives such as bromoaniline (BAN), O-phenylenediamine (PHD), 4-chloro-2-methylaniline (CMA), 4-chloroaniline (CAL), and m-toluidine (MTD) were taken in distilled water for DPA

https://doi.org/10.1021/acsomega.3c07158
ACS Omega 2024, 9, 2504−2518

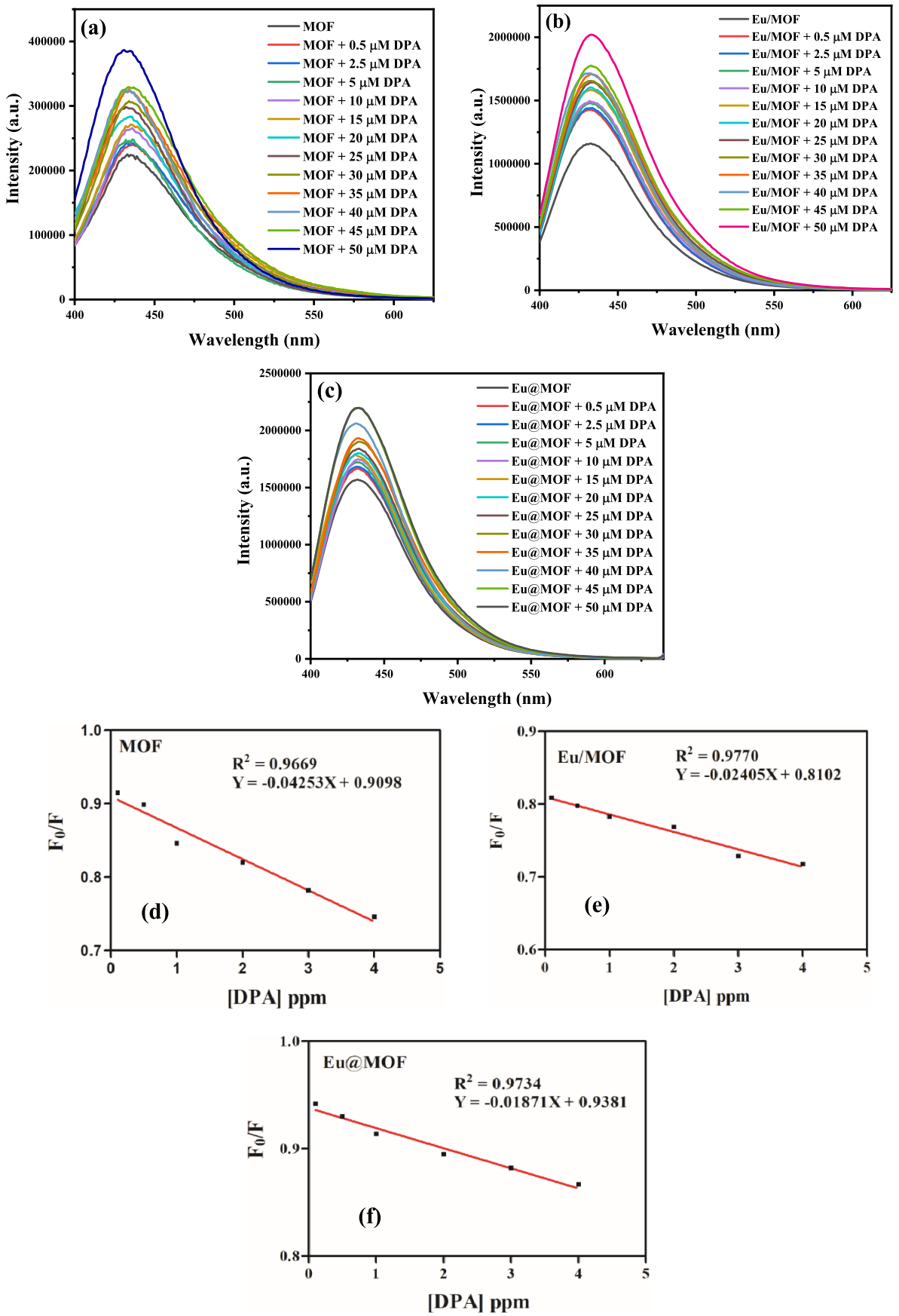

Figure 9. (a–c) Fluorometric detection of DPA dispersed in water with spiked $Eu(NO_3)_3.5H_2O$ concentrations at an excitation of 365 nm for MOF, Eu/MOF, and Eu@MOF, respectively; (d–f) Stern–Volmer plots for LOD measurement of DPA with good linearity (R^2).

https://doi.org/10.1021/acsomega.3c07158
ACS Omega 2024, 9, 2504–2518

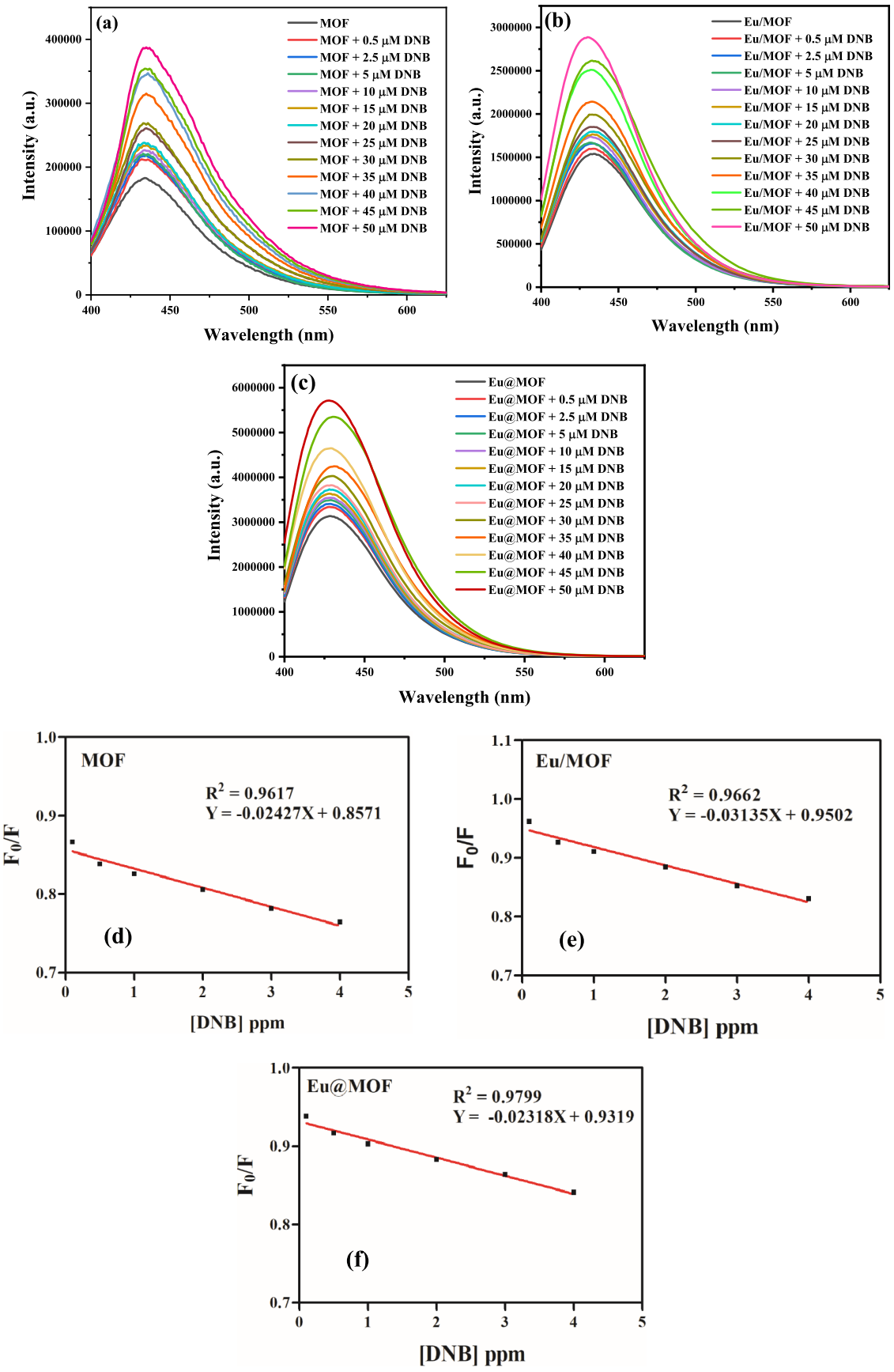

Figure 10. (a–c) Fluorometric detection of DNB dispersed in water with spiked $Eu(NO_3)_3.5H_2O$ concentrations at an excitation of 365 nm for MOF, Eu/MOF, and Eu@MOF, respectively; (d–f) Stern–Volmer plots for LOD measurement of DNB with good linearity (R^2 value).

https://doi.org/10.1021/acsomega.3c07158
ACS Omega 2024, 9, 2504–2518

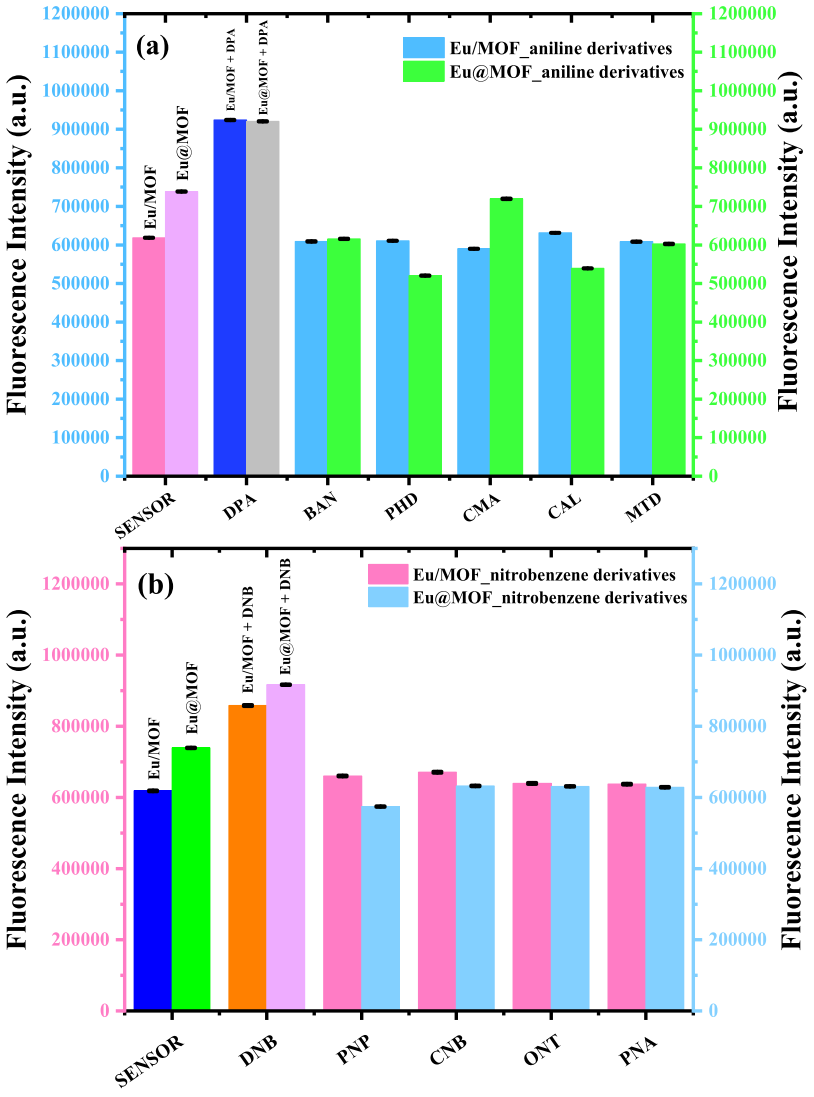

Figure 11. (a, b) Fluorescence response (error bar diagrams) of Eu/MOF and Eu@MOF sensors with various spiked aniline derivatives and nitrobenzene derivatives in distilled water at 365 nm excitation for DPA and DNB selectivity tests, respectively.

selectivity test. Nitrobenzene derivatives such as 4-nitrophenol (PNP), 1-chloro-3-nitrobenzene (CNB), 2-nitrotoluene (ONT), and p-nitroaniline (PNA) were taken in distilled water for DNB selectivity test. The concentrations of analytes diphenylamine (DPA) and dinitrobenzene (DNB) and aniline and nitrobenzene derivatives were taken to be 50 μM, 20 μL. The Eu^{3+}-incorporated MOF concentration was 0.2 mg/mL, 20 μL. It was found that the sensors exhibit the highest turn-on fluorescence sensing for DPA and DNB than their derivatives, which confirms the highly selective nature of the sensors toward DPA and DNB detection in distilled water as shown in Figure 11a,b.

The fluorescence and water stability of the sensors were confirmed by fluorescence and XRD analysis. The fluorescence readings were taken at a similar concentration of 0.2 mg/mL (200 μL) for all three MOFs with an excitation of 365 nm. It was observed that the Eu^{3+}-incorporated MOFs exhibit good fluorescence stability in water as could be seen from fluorescence spectral analysis (Figure S3a) as there is no decrease in the fluorescence intensities of the europium-incorporated sensors than the freshly prepared one even after exposure to water for a week. An increase in the fluorescence emission intensity for all the sensors could be observed after 1 week exposure to water which confirms the excellent fluorescent behavior of the materials (Figure S3a) with intact structural integrity, which was confirmed from PXRD analysis (Figure S3b). From XRD analysis, no change in the 2θ positions of the Eu^{3+}-incorporated MOFs was observed even after 2 weeks of immersion in water, which confirms the stability of the sensors in water (Figure S3b). Considering good water and fluorescence stability, high selectivity and sensitivity, and highly luminescent properties, the sensors can be considered as highly efficient in nature for fluorometric DPA and DNB detection in water. The sensor Eu/MOF exhibited better performance for DPA, and Eu@MOF exhibited better performance for DNB detection, which were confirmed from LOD measurements. A comparison table (Table S1) of different types of sensors for DPA and DNB sensing is provided in Supplementary Data (SD).

3.3. Real Sample Analysis. To check the future applicability of the sensor toward real sample analysis, the fluorescence sensing activity was carried out in industrial water samples with spiked DNB concentrations using the standard addition method. Five different concentrated solutions of 0.5, 5, 15, 25, and 35 μM DNB in industrial water were taken, and

https://doi.org/10.1021/acsomega.3c07158
ACS Omega 2024, 9, 2504−2518

Table 3. Fluorescence Sensing Study with the Aqueous Apple Extract Solution[a]

samples	sensor	added [DPA] (μM)	found [DPA] (μM)	recovery (%)	RSD (%)
aqueous apple extract solution	Eu/MOF	0.5	0.45	90.0	0.12
		5	5.05	101.1	0.05
		15	14.26	95.1	0.06
		25	23.50	94.0	0.04
		35	35.69	101.9	0.08
	Eu@MOF	0.5	0.4	80.0	0.07
		5	5.26	105.3	0.05
		15	13.27	88.5	0.01
		25	24.69	98.7	0.03
		35	34.57	96.3	0.02

[a]The results are executed as mean value of three measurements.

fluorescence measurements were recorded using a fluorescence spectrophotometer. The found DNB concentration was almost similar to the spiked amounts with a good recovery rate which confirms the highly effective nature of the sensors toward real sample analysis (Table 2).

The sensors were also used for DPA detection in apple skin. Since apples are stored in DPA as a preservative for a longer lifetime, there is the possibility of having very little DPA content in apple skin. Consuming DPA-containing apples on a daily basis may deteriorate the health of human beings. Therefore, some apples were brought from the market for DPA analysis in apple skin using the sensors. It was found from experimental analysis using HRMS that only a few apples that were examined contained a very small amount of DPA. To know the actual DPA content in an apple, spectrophotometric calibration method and high-resolution mass spectrometry (HRMS) analysis were performed. spectrophotometric analysis confirms that the apple extract (outer layer) in water shows a similar absorption peak at 280 nm as that of standard DPA solution in water (0.005 ppm), which confirms the presence of DPA in apple skin (Figure S4a). From the spectrophotometric calibration curve (Figure S4b,c), it was found that a very small amount of 0.0052 ppm of DPA was present in one apple's outer layer under observation, which is not that toxic. High-resolution mass spectrometry (HRMS) analysis also confirms the presence of DPA in the aqueous apple extract sample as shown in Figure S5. Peel removed apple extract exhibited no DPA which was confirmed by HRMS analysis.

Therefore, fluorometric DPA detection in real aqueous apple extract samples (outer layer) was performed with large spiked DPA concentrations of 0.5, 5, 15, 25, and 35 μM to know the accuracy of the sensors to detect DPA in fruit samples. It was found that the obtained DPA amount in the aqueous apple extract solution is similar to that of the original DPA concentrations taken with a good recovery percentage (Table 3). This confirms that the sensors can be used effectively for fluorometric DPA sensing in aqueous apple extract samples with high accuracy.

The calculated relative standard deviations (RSD) values are very small, suggesting that the instrumental performance for DPA and DNB detection is satisfactory.

The Eu^{3+}-incorporated Zr-MOFs sensors were used for reversibility and recyclability test after sensing analysis, and we found that the recovered catalysts exhibit strong fluorescence emissions even after three recycling runs, which confirms the high stability of the sensors for diphenylamine and dinitrobenzene detection in water (Figure S8 of Appendix A Supplementary Data). A little enhancement in the fluorescence intensity of the sensors after each cycle could be observed in the detection process, which may be because of the interaction between the Eu^{3+} metal ion with available electron-rich nitrogen atoms in diphenylamine and dinitrobenzene due to multiple uses of the recovered catalysts with time. Still, the detection performance remains intact for the sensors.

3.4. Sensing Mechanism Study. To understand the sensing mechanism between the sensor and the analyte, spectroscopic analyses were performed. Photoluminescence study confirms that ligand to metal charge transfer (LMCT) transitions in Eu^{3+}-incorporated Zr-MOFs are more dominant than lanthanide metal emissions (LME), executing strong luminescence, as discussed above. The synergistic effect of lanthanide metal ion and MOF interactions enhances their detection ability toward new guest molecules on the highly uniform porous MOF surface. Considering the good detection capability of the Eu@MOF sensor for DNB and the Eu/MOF sensor for DPA, the sensing mechanism was studied for the sensors toward the respective analytes.

The sensor Eu@MOF seemed to exhibit an inner filter effect toward fluorometric turn-on sensing of DNB as confirmed by spectrophotometric analysis. The absorption band of the Eu@MOF sensor was found to exhibit partial overlapping with the emission band of the analyte DNB, which confirms the inner filter effect of the sensor for fluorometric detection of DNB in water (Figure 12a). Fluorescence lifetime measurements were found to be constant for Eu@MOF before and after analyte addition, which confirms no dynamic quenching effect of the sensor toward DNB detection (Figure 12b). Additionally, no change in the PXRD measurements was observed, which confirms that no new complex has formed between the Eu@MOF sensor and the analyte DNB (Figure 12c).

The sensor Eu/MOF also exhibited the inner filter effect toward fluorometric turn-on sensing of DPA in water as there is complete overlapping of the absorption band of the Eu/MOF sensor with the emission band of the analyte DPA (Figure 12d). Fluorescence lifetimes for the sensor before and after analyte addition seemed to be constant, which proves no dynamic quenching effect between the sensor and the analyte (Figure 12e). A change in the structural integrity of the Eu/MOF sensor after DPA addition could be observed from PXRD measurements, which may be due to some possible structural changes during sensor and analyte interaction (Figure 12f).

4. CONCLUSIONS

The Eu^{3+} -incorporated MOFs were synthesized successfully using solvothermal synthesis methods. Europium metal ions are homogeneously distributed on the highly porous MOF surface

https://doi.org/10.1021/acsomega.3c07158
ACS Omega 2024, 9, 2504−2518

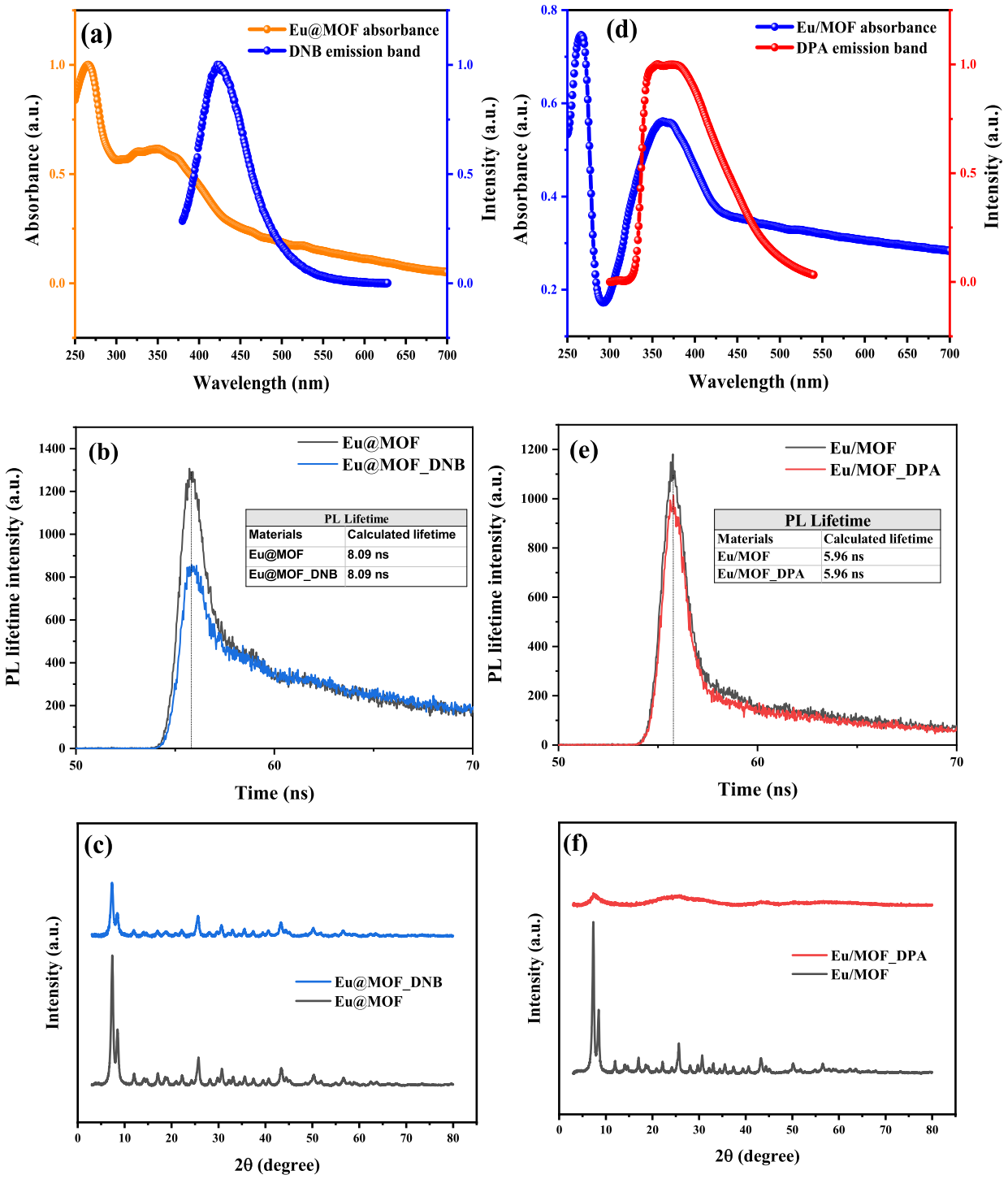

Figure 12. (a) Absorbance of Eu@MOF sensor and emission band of analyte DNB; (b) Fluorescence lifetime spectra for the Eu@MOF sensor before and after analyte (DNB) addition; (c) PXRD analysis of the Eu@MOF sensor before and after analyte (DNB) addition; (d) Absorbance of the Eu/MOF sensor and emission band of analyte DPA; (e) Fluorescence lifetime spectra for the Eu/MOF sensor before and after analyte (DPA) addition; and (f) PXRD analysis of the Eu/MOF sensor before and after analyte (DPA) addition.

which enhances the optical properties of the MOFs without changing their structural integrity. DFT analysis also confirms the intact structural integrity, stability, and enhancement in the luminescent properties via charge transfer interactions of the Eu^{3+}-incorporated MOFs. The sensors exhibited distinct turn-on fluorescence sensing for analytes DPA and DNB detection in water with good fluorescence stability and high selectivity and sensitivity. The sensors were used to see their applicability toward real sample analysis and were found effective toward DPA and DNB detection in real water samples (industrial water and aqueous apple extract samples) with good detection sensitivity. The Eu@MOF sensor exhibited excellent detection ability for DNB in water with LOD 0.652 ppm and a Stern–Volmer constant (K_{sv}) of 2.4×10^{-2} M^{-1}. Otherwise, the sensor Eu/MOF exhibited excellent DPA detection ability in water with a LOD of 0.698 ppm, and the Stern–Volmer constant (K_{sv})

https://doi.org/10.1021/acsomega.3c07158
ACS Omega 2024, 9, 2504−2518

obtained was 2.9×10^{-2} M^{-1}. Both the sensors exhibited the inner filter effect toward turn-on fluorometric sensing of DNB and DPA. The detection capacity of Eu^{3+}-incorporated MOFs was found better than the sole MOF. The incorporation of Eu^{3+} metal ions into the amino-functionalized Zr-MOF enhances the electronic stability of the materials, elongating their fluorescence lifetime with enhanced fluorescence sensing ability to detect hazardous organic compounds for environmental remediation.

■ ASSOCIATED CONTENT

Supporting Information

The Supporting Information is available free of charge at https://pubs.acs.org/doi/10.1021/acsomega.3c07158.

Synthesis of NH_2−UiO-66 MOF, general information and instrumentation, EDX of the synthesized materials, MS measurements for europium metal ions, experimental regarding fluorescence and water stability of the sensors, DPA content measurements in apples, spectrophotometric analysis, high-resolution mass spectrometry analysis, error bar diagrams for fluorometric detection of DPA and DNB in water using the sensors, reversibility and recyclability tests of the sensors toward diphenylamine and dinitrobenzene detection, and comparison of different sensors for DPA and DNB detection (PDF)

■ AUTHOR INFORMATION

Corresponding Author

Lakshi Saikia − *Advanced Materials Group, Materials Sciences and Technology Division, CSIR-North East Institute of Science & Technology, Jorhat, Assam 785006, India; Academy of Scientific and Innovative Research (AcSIR), Ghaziabad 201002, India;* orcid.org/0000-0003-0892-7233; Email: l.saikia@gmail.com, lsaikia@neist.res.in

Authors

Karanika Sonowal − *Advanced Materials Group, Materials Sciences and Technology Division, CSIR-North East Institute of Science & Technology, Jorhat, Assam 785006, India; Academy of Scientific and Innovative Research (AcSIR), Ghaziabad 201002, India*

Sanmilan Jyoti Kalita − *Advanced Materials Group, Materials Sciences and Technology Division, CSIR-North East Institute of Science & Technology, Jorhat, Assam 785006, India; Academy of Scientific and Innovative Research (AcSIR), Ghaziabad 201002, India*

Siddhartha K. Purkayastha − *Department of Chemistry, Assam Don Bosco University, Sonapur 782402, India*

Juri Goswami − *Jorhat Institute of Science and Technology, Jorhat, Assam 785010, India*

Purashri Basyach − *Advanced Materials Group, Materials Sciences and Technology Division, CSIR-North East Institute of Science & Technology, Jorhat, Assam 785006, India; Academy of Scientific and Innovative Research (AcSIR), Ghaziabad 201002, India*

Riya Das − *Advanced Materials Group, Materials Sciences and Technology Division, CSIR-North East Institute of Science & Technology, Jorhat, Assam 785006, India*

Abhishek Borborah − *Advanced Materials Group, Materials Sciences and Technology Division, CSIR-North East Institute of Science & Technology, Jorhat, Assam 785006, India*

Ankur K. Guha − *Advanced Computational Chemistry Centre, Cotton University, Guwahati, Assam 781001, India;* orcid.org/0000-0003-4370-8108

Complete contact information is available at: https://pubs.acs.org/10.1021/acsomega.3c07158

Notes

The authors declare no competing financial interest.

■ ACKNOWLEDGMENTS

The authors are thankful to the Director of CSIR-NEIST, Jorhat, for his kind support and allowance to publish the research work. K.S. acknowledges the University Grants Commission (UGC)-New Delhi for CSIR-UGC (NET) fellowship and L.S. acknowledges the in-house project OLP-2078 for financial support. Authors are thankful to the analytical division for providing instrumental facilities.

■ REFERENCES

(1) Falcaro, P.; Ricco, R.; Yazdi, A.; Imaz, I.; Furukawa, S.; Maspoch, D.; Ameloot, R.; Evans, J. D.; Doonan, C. J. Application of Metal and Metal Oxide Nanoparticles@MOFs. *Coord. Chem. Rev.* **2016**, *307*, 237−254.

(2) Wang, J.; Jiu, J.; Araki, T.; Nogi, M.; Sugahara, T.; Nagao, S.; Koga, H.; He, P.; Suganuma, K. Silver Nanowire Electrodes: Conductivity Improvement without Post-Treatment and Application in Capacitive Pressure Sensors. *Nanomicro Lett.* **2015**, *7* (1), 51−58.

(3) Yang, Z.; Li, Z.; Xu, M.; Ma, Y.; Zhang, J.; Su, Y.; Gao, F.; Wei, H.; Zhang, L. Controllable Synthesis of Fluorescent Carbon Dots and Their Detection Application as Nanoprobes. *Nano-Micro Lett.* **2013**, *5*, 247−259.

(4) Fang, X.; Zong, B.; Mao, S. Metal−Organic Framework-Based Sensors for Environmental Contaminant Sensing. *Nano-Micro Lett.* **2018**, *10*, 64.

(5) Willner, M. R.; Vikesland, P. J. Nanomaterial Enabled Sensors for Environmental Contaminants. *J. Nanobiotechnol.* **2018**, *16*, 95.

(6) Malhotra, R.; Patel, V.; Pedro Vaqué, J.; Silvio Gutkind, J.; Rusling, F.; J. Ultrasensitive Electrochemical Immunosensor for Oral Cancer Biomarker IL-6 Using Carbon Nanotube Forest Electrodes and Multilabel Amplification. *Anal. Chem.* **2010**, *82* (8), 3118−3123.

(7) Bo, Z.; Yuan, M.; Mao, S.; Chen, X.; Yan, J.; Cen, K. Decoration of Vertical Graphene with Tin Dioxide Nanoparticles for Highly Sensitive Room Temperature Formaldehyde Sensing. *Sens. Actuators B Chem.* **2018**, *256*, 1011−1020.

(8) Liu, S.; Zhang, J.; Tu, W.; Bao, J.; Dai, Z. Using Ruthenium Polypyridyl Functionalized ZnO Mesocrystals and Gold Nanoparticle Dotted Graphene Composite for Biological Recognition and Electrochemiluminescence Biosensing. *Nanoscale* **2014**, *6* (4), 2419−2425.

(9) Wang, G.; Chen, Z.; Chen, L. Mesoporous Silica-Coated Gold Nanorods: Towards Sensitive Colorimetric Sensing of Ascorbic Acid via Target-Induced Silver Overcoating. *Nanoscale* **2011**, *3* (4), 1756−1759.

(10) Cha, J.; Han, J. I.; Choi, Y.; Yoon, D. S.; Oh, K. W.; Lim, G. DNA Hybridization Electrochemical Sensor Using Conducting Polymer. *Biosens. Bioelectron.* **2003**, *18* (10), 1241−1247.

(11) Goswami, J.; Rohman, S. S.; Guha, A. K.; Basyach, P.; Sonowal, K.; Borah, S. P.; Saikia, L.; Hazarika, P. Phosphoric Acid Assisted Synthesis of Fluorescent Carbon Dots from Waste Biomass for Detection of Cr(VI) in Aqueous Media. *Mater. Chem. Phys.* **2022**, *286*, No. 126133.

(12) Gogoi, M.; Borborah, A.; Saikia, L. Development of Quantum Dot Complex for Selective Detection of Pyrophosphate Anion with Fluorescence Quenching. *Bull. Mater. Sci.* **2021**, *44* (4), 264.

(13) Sonowal, K.; Saikia, L. Functional Groups Assisted-Photo-induced Electron Transfer-Mediated Highly Fluorescent Metal-Organic Framework Quantum Dot Composite for Selective Detection of Mercury (II) in Water. *J. Environ. Sci. (China)* **2023**, *126*, 531−544.

(14) Karthik, R.; Karikalan, N.; Chen, S. M.; Vinoth Kumar, J.; Karuppiah, C.; Muthuraj, V. Assessment of Divergent Functional Properties of Seed-like Strontium Molybdate for the Photocatalysis and Electrocatalysis of the postharvest Scald Inhibitor diphenylamine. *J. Catal.* **2017**, *352*, 606−616.
(15) Umesh, N. M.; Antolin Jesila, J.; Wang, S. F.; Shalini Devi, K. S.; Vishnu, N. Highly Selective Electrochemical Detection of diphenylamine in Apple Samples Using Rod Shaped $CuCo_2O_4$ Derived from Bimetallic Organic Frameworks. *Microchem. J.* **2021**, *165*, No. 106146.
(16) Afkhami, A.; Bahram, M.; Gholami, S.; Zand, Z. Micell-Mediated Extraction for the spectrophotometric Determination of Nitrite in Water and Biological Samples Based on Its Reaction with p-Nitroaniline in the Presence of diphenylamine. *Anal. Biochem.* **2005**, *336* (2), 295−299.
(17) Han, M. L.; Xu, G. W.; Li, D. S.; Azofra, L. M.; Zhao, J.; Chen, B.; Sun, C. A Terbium-Organic Framework Material for Highly Sensitive Sensing of Fe^{3+} in Aqueous and Biological Systems: Experimental Studies and Theoretical Analysis. *ChemistrySelect* **2016**, *1* (13), 3555−3561.
(18) Yang, L. Z.; Wang, J.; Kirillov, A. M.; Dou, W.; Xu, C.; Fang, R.; Xu, C. L.; Liu, W. S. 2D Lanthanide MOFs Driven by a Rigid 3,5-Bis(3-Carboxy-Phenyl)Pyridine Building Block: Solvothermal Syntheses, Structural Features, and Photoluminescence and Sensing Properties. *CrystEngComm* **2016**, *18* (34), 6425−6436.
(19) Zeng, G.; Xing, S.; Wang, X.; Yang, Y.; Ma, D.; Liang, H.; Gao, L.; Hua, J.; Li, G.; Shi, Z.; Feng, S. 3d−4f Metal−Organic Framework with Dual Luminescent Centers That Efficiently Discriminates the Isomer and Homologues of Small Organic Molecules. *Inorg. Chem.* **2016**, *55* (3), 1089−1095.
(20) Li, Z.; Zhan, Z.; Jia, Y.; Li, Z.; Hu, M. A Water-Stable Europium-MOF as a Multifunctional Luminescent Sensor for Some Inorganic Ions and Dichloromethane Molecule. *Ind. Eng. Chem. Res.* **2021**, *97*, 180−187.
(21) Gao, R.-C.; Guo, F.-S.; Bai, N.-N.; Wu, Y.-L.; Yang, F.; Liang, J.-Y.; Li, Z.-J.; Wang, Y.-Y. Two 3D Isostructural Ln(III)-MOFs: Displaying the Slow Magnetic Relaxation and Luminescence Properties in Detection of Nitrobenzene and $Cr_2O_7^{2-}$. *Inorg. Chem.* **2016**, *55* (21), 11323−11330.
(22) Xu, H.; Fang, M.; Cao, C. S.; Qiao, W. Z.; Zhao, B. Unique (3,4,10)-Connected Lanthanide-Organic Framework as a Recyclable Chemical Sensor for Detecting Al^{3+}. *Inorg. Chem.* **2016**, *55* (10), 4790−4794.
(23) Wen, G.-X.; Wu, Y.-P.; Dong, W.-W.; Zhao, J.; Li, D.-S.; Zhang, J. An Ultrastable Europium(III)−Organic Framework with the Capacity of Discriminating Fe^{2+}/Fe^{3+} Ions in Various Solutions. *Inorg. Chem.* **2016**, *55* (20), 10114−10117.
(24) Liu, C.; Yan, B. Zeolite-Type Metal Organic Frameworks Immobilized Eu3+ for Cation Sensing in Aqueous Environment. *J. Colloid Interface Sci.* **2015**, *459*, 206−211.
(25) Yang, C.-X.; Ren, H.-B.; Yan, X.-P. Fluorescent Metal−Organic Framework MIL-53(Al) for Highly Selective and Sensitive Detection of Fe^{3+} in Aqueous Solution. *Anal. Chem.* **2013**, *85* (15), 7441−7446.
(26) Pan, Y.; Wang, J.; Guo, X.; Liu, X.; Tang, X.; Zhang, H. A New Three-Dimensional Zinc-Based Metal-Organic Framework as a Fluorescent Sensor for Detection of Cadmium Ion and Nitrobenzene. *J. Colloid Interface Sci.* **2018**, *513*, 418−426.
(27) Stavila, V.; Talin, A. A.; Allendorf, M. D. MOF-Based Electronic and Opto-Electronic Devices. *Chem. Soc. Rev.* **2014**, *43*, 5994−6010.
(28) Sonowal, K.; Nandal, N.; Basyach, P.; Kalita, L.; Jain, S. L.; Saikia, L. Photocatalytic Reduction of CO_2 to Methanol Using Zr(IV)-Based MOF Composite with g-C_3N_4 Quantum Dots under Visible Light Irradiation. *J. CO2 Util.* **2022**, *57*, No. 101905.
(29) Zhou, S.; Tu, D.; Liu, Y.; You, W.; Zhang, Y.; Zheng, W.; Chen, X. Ultrasensitive Point-of-Care Test for Tumor Marker in Human Saliva Based on Luminescence-Amplification Strategy of Lanthanide Nanoprobes. *Adv. Sci.* **2021**, *8* (5), No. 2002657.
(30) Zeng, C. H.; Zheng, K.; Lou, K. L.; Meng, X. T.; Yan, Z. Q.; Ye, Z. N.; Su, R. R.; Zhong, S. Synthesis of Porous Europium Oxide Particles for Photoelectrochemical Water Splitting. *Electrochim. Acta* **2015**, *165*, 396−401.
(31) Xiaoxiong, Z.; Wenjun, Z.; Cuiliu, L.; Xiaohong, Q.; Chengyu, Z. Eu^{3+}-Postdoped UIO-66-Type Metal−Organic Framework as a Luminescent Sensor for Hg^{2+} Detection in Aqueous Media. *Inorg. Chem.* **2019**, *58* (6), 3910−3915.
(32) Perdew, J. P.; Burke, K.; Ernzerhof, M. Generalized Gradient Approximation Made Simple. *Phys. Rev. Lett.* **1996**, *77*, 3865−3868.
(33) Dolg, M.; Wedig, U.; Stoll, H.; Preuss, H. Energy-adjusted *ab initio* pseudopotentials for the first-row transition elements. *J. Chem. Phys.* **1987**, *86*, 866−872.
(34) Frisch, M. J.et al.*Gaussian 16, Revision A.03*; Gaussian, Inc.: Wallingford CT, 2016.
(35) Lu, T.; Chen, F. Multiwfn: A multifunctional wavefunction analyzer. *J. Comput. Chem.* **2012**, *33*, 580.
(36) Xie, X.-Z.; Zhang, Y.-R.; Wu, Y.-J.; Yin, X. B.; Xia, Y. Ligand Energy Staff Gauge for Antenna Effect Study within Metal-Organic Frameworks. *J. Phys. Chem. C* **2023**, *127* (2), 1220−1228.
(37) Zhang, Y.-R.; Xie, X.-Z.; Yin, X.-B.; Xia, Y. Flexible ligand−Gd dye-encapsulated dual-emission metal−Organic framework. *Dalton Trans.* **2022**, *51*, 17895−17901.
(38) Zhang, Y.-R.; Xie, X.-Z.; Yin, X.-B.; Xia, Y. Flexible ligand for Metal-Organic frameworks with simultaneous Large-Pore and antenna effect emission. *Chem. Eng. J.* **2022**, *443* (1), No. 136532.
(39) Xia, Y.-D.; Sun, Y.-Q.; Cheng, Y.; Xia, Y.; Yin, X.-B. Rational design of dual-ligand Eu-MOF for ratiometric fluorescence sensing Cu^{2+} ions in human serum to diagnose Wilson's disease. *Anal. Chim. Acta* **2022**, *1204*, No. 339731.
(40) Wei, W.; Zhang, Y. R.; Yin, X.-B.; Xia, Y. Multifunctional AIEgen-based luminescent metal−Organic frameworks with coordination-induced emission for chemical sensing. *New J. Chem.* **2022**, *46*, 9641−9649.

https://doi.org/10.1021/acsomega.3c07158
ACS Omega 2024, 9, 2504−2518